Geophys. J. Int. (1998) **133,** 363–378

Three-dimensional geometrical ray theory and modelling of transmitted seismic energy of data from the Nevada Test Site

How-Wei Chen

Institute of Seismology, Institute of Applied Geophysics, National Chung Cheng University, Min-Hsiung, Chia Yi, 621 *Taiwan, Republic of China.*
E-mail: seiswei@eq.ccu.edu.tw

Accepted 1997 November 17. Received 1997 November 12; in original form 1997 June 17

SUMMARY

This paper presents a geometrically based algorithm for computing synthetic seismograms for energy transmitted through a 3-D velocity distribution. 3-D ray tracing is performed to compute the traveltimes and geometrical spreading (amplitude). The formulations of both kinematic and dynamic ray-tracing systems are presented. The two-point ray-tracing problem is solved by systematically updating the initial conditions and adjusting the ray direction until the ray intersects the specified endpoint. The amount of adjustment required depends on the derivatives of the position with respect to the given starting angles between consecutive rays. The algorithm uses derivatives to define the steepest-descent direction and to update the initial directions. The convergence rate depends on the complexity of the model.

Test seismograms compare favourably with those from a 2-D asymptotic ray theory algorithm and a 3-D Gaussian-beam algorithm. The algorithm is flexible in modelling arbitrary source and recorder geometries for various smoothly varying 3-D velocity distributions. The algorithm is further tested by simulating surface-to-tunnel vibroseis field data. Shear waves as well as compressional waves may be approximately included. Application of the algorithm to a data set from the Rainier Mesa of the Nevada Test Site produced a good fit to the transmitted (first arrival) traveltimes and amplitudes, with approximately 15 per cent variation in the local 3-D velocity.

Key words: 3-D structure, amplitude, ray tracing, synthetic seismograms, traveltime.

INTRODUCTION

In seismic exploration and earthquake seismology, numerical modelling is a practical tool to understand physical seismic-wave propagation within complex 2-D and 3-D subsurface structures. The growing interest in wave propagation simulation is widely and successfully applied to understand various wavefield phenomena generated by a passive source (earthquake) or a controlled source (dynamite). Seismic data are being recorded more densely and in increasingly diverse array patterns. From field observations it is increasingly apparent that the Earth, in most regions of seismic interest, particularly those that are tectonically active, is significantly heterogeneous in all three spatial dimensions. In the past ten years, there has been a changing trend in modelling algorithms, from 1-D and 2-D to 3-D simulation of wave propagation phenomena. Numerical modelling is potentially valuable in both survey design and data interpretation.

Synthetic seismogram simulation is especially important in describing wave propagation effects due to changes in model geometry and velocity structures. The numerical modelling techniques may include ray theory (Julian & Gubbins 1977; Lee & Stewart 1981), Kirchhoff–Helmholtz integration (Trorey 1970; Hilterman 1970), a hybrid analytic–numerical algorithm (Mikhailenko 1984), 3-D slowness integration (Burdick & Salvado 1986), 3-D Fourier transformation (McMechan, Wen & Morales 1988), wavenumber–frequency integration (Bard & Buchon 1980a,b), finite differences (Mufti 1990), finite elements (Smith 1975), the WKBJ method (Chapman 1978; Sinton & Frazer 1982) and phase integration (Frazer & Phinney 1980).

Previous work on 3-D ray-based modelling ranges from traveltime computing based on shooting and bending methods (e.g. Julian & Gubbins 1977; Um & Thurber 1987), through geometrical spreading (*cf*. Wesson 1970) to computation of synthetic seismograms. The methods involve searching for a ray and calculating the minimum traveltime and ray path between two prescribed locations. The high-frequency approximation of ray-theory synthetic seismograms has been developed by a variety of methods including Gaussian-beam and paraxial-ray approximations (Červený & Pšenčík 1983; Červený & Klimeš 1984; Beydoun & Keho 1987), and dynamic ray tracing (Červený & Hron 1980; Azbel *et al*. 1984; Červený,

Klimeš & Pšenčík 1988). The basic problem of numerical ray-theory modelling of seismic wavefields in a 3-D structure consists of two-point ray tracing. Two-point ray-tracing problems may be solved by using Fermat's principle (Waltham 1988), by solving a finite system of equations (Pereyra 1992; Hanyga 1988), by using point-to-curve tracing (Hanyga 1996) and by shooting in the normalized ray domain (Bulant 1996).

A scheme based on the expanding-wave-front theory was recently developed as an alternative to conventional ray-path computing. Reshef & Kosloff (1986) proposed the initial idea on the basis of the eikonal equation. Vidale (1988, 1990) presented a finite-difference scheme to calculate the traveltime at all corners of cubic cells. Van Trier & Symes (1991) proposed an improved version for solving the eikonal equation by an upwind finite-difference scheme. Podvin & Lecomte (1991) presented a parallel version of their finite-difference calculation. Dellinger (1991) later applied it to anisotropic media. Qin *et al.* (1992) further improved the algorithm by calculating the traveltime along expanding wave fronts rather than along the expanding squares.

On the basis of Huygens' principle and the algorithm of Dijkstra (1959), Nakanishi & Yamaguchi (1986), Moser (l991) and Saito (1989, 1990) developed efficient methods for finding the shortest ray-path tracing on a model consisting of uniform-velocity cells. These investigators suggested that the earth model can be parametrized into a network of nodes on the boundaries of block cells. Calculating the traveltime from a source to all nodes is reduced to a problem of sparse graphic searching. Cao & Greenhalgh (1993), Fischer & Lees (1993) and Klimeš & Kvasnicka (1994) developed similar techniques for improving the efficiency of shortest-path ray tracing with error analysis. Kao & Chen (1996) presented a parallel implementation of a similar algorithm, using irregular polygonal cells for 2-D models and discrete convex blocks bounded by polyhedral facets for 3-D models, on massively parallel processors. Pereyra (l996) presented a different distributed computational strategy for 3-D ray tracing and traveltime inversion for large-scale problems. As an alternative, the wave-front construction technique was introduced by Vinje, Iversen & Gjoystdal (1993). Ettrich & Gajewaki (1996) later applied the algorithm to a 2-D Kirchhoff-style pre-stack depth migration.

Most of the methods described above pertain mainly to the theoretical and computational aspects of seismic-wave propagation in complex structures and thus are occasionally complicated to implement. To date, however, there are few published reports on the application of 3-D synthetic seismograms to the modelling of 3-D field data. The major contribution of the present paper is to develop a relatively simple and straightforward geometrically based algorithm and to apply it to a real data set.

THEORY

The synthetic seismograms are high-frequency approximations computed for transmitted (refracted) energy in a 3-D velocity distribution. The approach is purely geometrical. The major steps involve model building, two-point seismic ray tracing using a shooting technique; the calculation of geometrical spreading, source and recorder directivity, and the free-surface conversion coefficient (if required); resolution of the final response vector into vertical and horizontal components; and convolution of the impulse response with a source time function.

Model building involves specifying a small number of points for each boundary and velocity. The input velocity points are interpolated with a polynomial to provide a smooth, piecewise continuous interpolation and the derivatives needed in the ray tracing. The traveltime and geometrical spreading are calculated by a 3-D ray tracer. A brief description of the traveltime and ray-path computation is given in Appendix A. The algorithm follows the unified formulation of Pereyra, Lee & Keller (1980) as summarized by Lee & Stewart (1981). Seven equations (A3) are solved by numerical integration using the subroutine DEROOT of Shampine & Gordon (1975). Amplitude computation is based on the simplified approach of Wesson (1970) and May & Hron (1978), presented below and in Appendix B.

An important application of seismic ray tracing is tracing a ray from point A to point B when point B is located on the surface $z = 0.0$ km (Fig. 1). In this case, point A corresponds to an earthquake hypocentre and point B to a seismic station. Let $[X(\alpha, \beta), Y(\alpha, \beta), 0]$ be the point at which a ray leaving point A with azimuth α and take-off angle β intersects the surface. The problem thus involves solving the non-linear equations $X(\alpha^*, \beta^*) = X_B$ and $Y(\alpha^*, \beta^*) = Y_B$, where $(X_B, Y_B, 0)$ are the coordinates of point B and (α^*, β^*) are the initial directions at point A of the ray joining points A and B. In the case of the two-point problem, one may begin initially by assuming the ray direction at one point and subsequently (1) solving the initial-value problem and (2) adjusting the

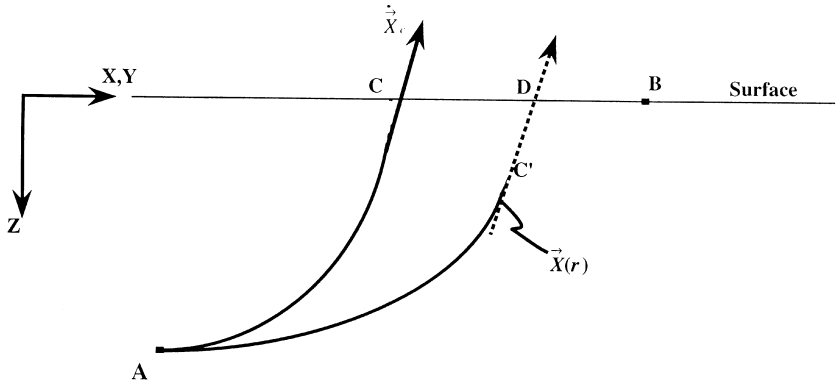

Figure 1. An arbitrary ray through a seismic coordinate system. The coordinate systems, source and station locations, and position vectors used in the two-point ray tracing are illustrated.

initial ray direction until a ray that intersects the second point is found. The shooting method can be performed without using the derivatives of changes in position along a ray to adjust the initial ray directions, but fewer iterations of the above steps (1) and (2) may be required if $\partial x(s)/\partial\alpha$, $\partial y(s)/\partial\alpha$, $\partial x(s)/\partial\beta$, and $\partial y(s)/\partial\beta$ are known. It is straightforward to obtain these derivatives for a given α and β. The formulation for computing derivatives on the basis of a dynamic ray-tracing algorithm is presented in Appendix B.

Consider tracing a ray from point A which intersects the surface at point C and has a path length of S between A and C. The initial direction of the ray is perturbed by $d\alpha$ and $d\beta$ such that after travelling a distance S from point A the new ray has reached point C′. Let $(X_C, Y_C, 0)$ be the coordinates of point C. By solving eqs B3, the derivatives $(\partial\mathbf{X}/\partial\alpha)|_C$ and $(\partial\mathbf{Y}/\partial\alpha)|_C$ are known and we can approximate the position of point C′ by

$$
\begin{aligned}
x_{C'} &\approx X_C + \left.\frac{\partial x}{\partial\alpha}\right|_C d\alpha + \left.\frac{\partial x}{\partial\beta}\right|_C d\beta,\\
y_{C'} &\approx Y_C + \left.\frac{\partial y}{\partial\alpha}\right|_C d\alpha + \left.\frac{\partial y}{\partial\beta}\right|_C d\beta,\\
z_{C'} &\approx \left.\frac{\partial z}{\partial\alpha}\right|_C d\alpha + \left.\frac{\partial z}{\partial\beta}\right|_C d\beta.
\end{aligned}
\tag{1}
$$

Now consider the parametric expression for the line passing through point C′ in the direction of the ray at C, $\dot{\mathbf{X}}_C$:

$$
\mathbf{X}(r) = \mathbf{X}_{C'} + r\dot{\mathbf{X}}_C, \tag{2}
$$

where r denotes a parameter representing distance along the line from C′. The point at which this line intersects the surface is, to first order, the same as the point D with coordinates $(X_D, Y_D, 0)$ at which the perturbed ray intersects the surface. Solving the equations

$$
\begin{aligned}
X_D(r) &= x_{C'} + r\dot{x}_C,\\
Y_D(r) &= y_{C'} + r\dot{y}_C,\\
0 &= z_{C'} + r\dot{z}_C
\end{aligned}
\tag{3}
$$

and eliminating r yields

$$
\begin{aligned}
X_D(r) &= x_{C'} + \frac{\dot{x}_C}{\dot{z}_C}\dot{z}_{C'},\\
Y_D(r) &= y_{C'} + \frac{\dot{y}_C}{\dot{z}_C}z_{C'}.
\end{aligned}
\tag{4}
$$

When one substitutes for $x_{C'}$, $y_{C'}$, $z_{C'}$, this becomes

$$
\begin{aligned}
dX = X_D - X_C &= \left(\left.\frac{\partial x}{\partial\alpha}\right|_C + \frac{\dot{x}_C}{\dot{z}_C}\left.\frac{\partial z}{\partial\alpha}\right|_C\right)d\alpha\\
&\quad + \left(\left.\frac{\partial x}{\partial\beta}\right|_C + \frac{\dot{x}_C}{\dot{z}_C}\left.\frac{\partial z}{\partial\beta}\right|_C\right)d\beta,\\
dY = Y_D - Y_C &= \left(\left.\frac{\partial y}{\partial\alpha}\right|_C + \frac{\dot{y}_C}{\dot{z}_C}\left.\frac{\partial z}{\partial\alpha}\right|_C\right)d\alpha\\
&\quad + \left(\left.\frac{\partial y}{\partial\beta}\right|_C + \frac{\dot{y}_C}{\dot{z}_C}\left.\frac{\partial z}{\partial\beta}\right|_C\right)d\beta.
\end{aligned}
\tag{5}
$$

Note that in general, for rays originating at finite depth, $\dot{z}_C \neq 0$. Finally, we have the desired partial derivatives,

$$
\begin{aligned}
\frac{\partial X}{\partial\alpha} &= \frac{\partial x}{\partial\alpha} + \frac{\dot{x}}{\dot{z}}\frac{\partial z}{\partial\alpha} = W_7 + \frac{W_2}{W_6}W_{11},\\
\frac{\partial X}{\partial\beta} &= \frac{\partial x}{\partial\beta} + \frac{\dot{x}}{\dot{z}}\frac{\partial z}{\partial\beta} = W_{13} + \frac{W_2}{W_6}W_{17},\\
\frac{\partial Y}{\partial\alpha} &= \frac{\partial y}{\partial\alpha} + \frac{\dot{y}}{\dot{z}}\frac{\partial z}{\partial\alpha} = W_9 + \frac{W_4}{W_6}W_{11},\\
\frac{\partial Y}{\partial\beta} &= \frac{\partial y}{\partial\beta} + \frac{\dot{y}}{\dot{z}}\frac{\partial z}{\partial\beta} = W_{15} + \frac{W_4}{W_6}W_{17},
\end{aligned}
\tag{6}
$$

where all quantities on the right are to be evaluated at the endpoint $(X, Y, 0)$. The ray between a source and a recorder is found by iterative adjustment of the take-off angle and azimuth angle of the initial direction of a ray until the ray passes within a specified distance of the recorder. The convergence criterion of the two-point ray-tracing problem is controlled by the amount of change in position at the endpoint compared to the change from the previous iteration. The initial ray path is systematically perturbed until the difference between successive iterations is within the error limit. This provides the traveltime for the corresponding arrival in the synthetic seismogram. Once a ray path joining the source and receiver is found, it can be used to initiate a sequence of ray calculations for the neighbouring receiver positions. The algorithm may fail when the ray hits a caustic or a shadow zone. Under such a condition, the search can be performed by finding another ray, using appropriate control parameters.

The total amplitude associated with a source-to-recorder path is a combination of seven contributions. In the following sections, each contribution related to amplitude computation by means of a ray-based modelling algorithm is described. The complex total amplitude A_{total} can be written as

$$
A_{\text{total}} = \frac{A_S D_S D_R R}{G_i G_o}\prod_j T_j. \tag{7}
$$

Eq. (7) gives the amplitude; the power (energy) may be computed as amplitude squared. A_S represents the effective amplitude radiated by the source and implicitly contains a source-to-Earth coupling effect. Defining the source directivity in terms of the energy per unit area of the focal sphere, D_S and D_R are the source and receiver directivity factors, which contain the radiation pattern as a function of propagation angle. More details on radiation patterns can be found in Aki & Richards (1980) and Kennett (1983). G_i and G_o are the corresponding in-plane and out-of-plane geometric spreadings. The product of G_i and G_o represents the geometrical spreading of the ray tube. The plane-wave reflection coefficient R and the transmission coefficients T determine the energy partition across any velocity boundaries.

The effects of geometrical spreading on the wave energy and amplitude may be determined by the algorithm described by Wesson (1970). Neglecting scattering and attenuation, the intensity (and hence amplitude) is inversely proportional to the area of the wave front:

$$
\begin{aligned}
I = I_0\frac{d\Omega}{dA} = \frac{I_0}{\sin\beta}\Bigg|&\left(\frac{\partial y}{\partial\alpha}\frac{\partial z}{\partial\beta} - \frac{\partial z}{\partial\alpha}\frac{\partial y}{\partial\beta}\right)\frac{\partial x}{\partial s}\\
&+ \left(\frac{\partial z}{\partial\alpha}\frac{\partial x}{\partial\beta} - \frac{\partial x}{\partial\alpha}\frac{\partial z}{\partial\beta}\right)\frac{\partial y}{\partial s} + \left(\frac{\partial x}{\partial\alpha}\frac{\partial y}{\partial\beta} - \frac{\partial y}{\partial\alpha}\frac{\partial x}{\partial\beta}\right)\frac{\partial z}{\partial s}\Bigg|,
\end{aligned}
\tag{8}
$$

where I_0 is the initial intensity associated with the unit solid angle $d\Omega$ and I is the intensity associated with the element of area dA. This equation is valid for a 3-D medium through which rays can be traced. Moreover, eq. (8) can be interpreted geometrically as a bundle of rays emerging from a initial point with initial directions filling the infinitesimal solid angle $d\Omega$. Considering some particular ray within the bundle, and the infinitesimal area dA formed by the intersection of the bundle with a plane normal to the ray at a given point along the ray, dA is treated as an element of the wave-front surface at any particular arrival time. The computation of the infinitesimal area dA can be performed by determining the area of a parallelogram projected onto a plane normal to the propagation direction of the ray. The spreading calculation is implemented by tracing two additional rays at fixed (orthogonal) angle increments from the source-to-recorder ray. An infinitesimal solid angle $d\Omega$ and the calculated area dA enclosed by these three rays at a given point along the ray are thus defined. Three rays are used to approximate the ray tube. The geometrical spreading calculation can be further decomposed into the in-plane and out-of-plane geometrical spreadings by eqs (5) and (6) of May & Hron (1978).

A physical explanation of eq. (8) can be given as follows. If we define the effective spreading radius at a given point S_{eff} such that $S_{\text{eff}}^2 = dA/d\Omega$, then the energy at points along the ray decreases in proportion to $1/S_{\text{eff}}^2$ and the amplitude decreases in proportion to $1/S_{\text{eff}}$, if anelastic attenuation is neglected. For a medium of uniform velocity $S_{\text{eff}} = s$, the path length (and distance) from the initial point, and the corresponding $1/s^2$ decay of energy and $1/s$ decay of amplitude are well known.

Such an approach is advantageous in that the simplest form of spreading formulation (Wesson 1970) is directly implemented by interpreting the formula geometrically, without explicitly solving the 19 equations simultaneously for each ray (eqs B3). With this simplification, we have to solve seven ordinary differential equations (eqs A3) simultaneously. This algorithm, however, does not resolve the problem of infinite amplitudes predicted for caustics, where the area of the ray tube goes to zero. Eq. (8) must, obviously, be restricted to rays for which $\sin\beta \neq 0$. Such a restriction, though relatively insignificant, may be overcome by redefining $\partial\alpha$ and $\partial\beta$ for such rays, perhaps via a permutation of the axes, for example from (x, y, z) to (z, x, y).

The angle-dependent reflection and transmission coefficients related to seismic plane waves incident on a plane interface are based on Červený & Ravindra (1971), pp. 58–70. Both reflected and refracted *P-SV* (16 different coefficients) and *SH* (four coefficients) waves for a single interface (*cf.* Fig. 2.8 of Červený & Ravindra 1971) are included explicitly in the computation. All the conversion coefficients and reflection

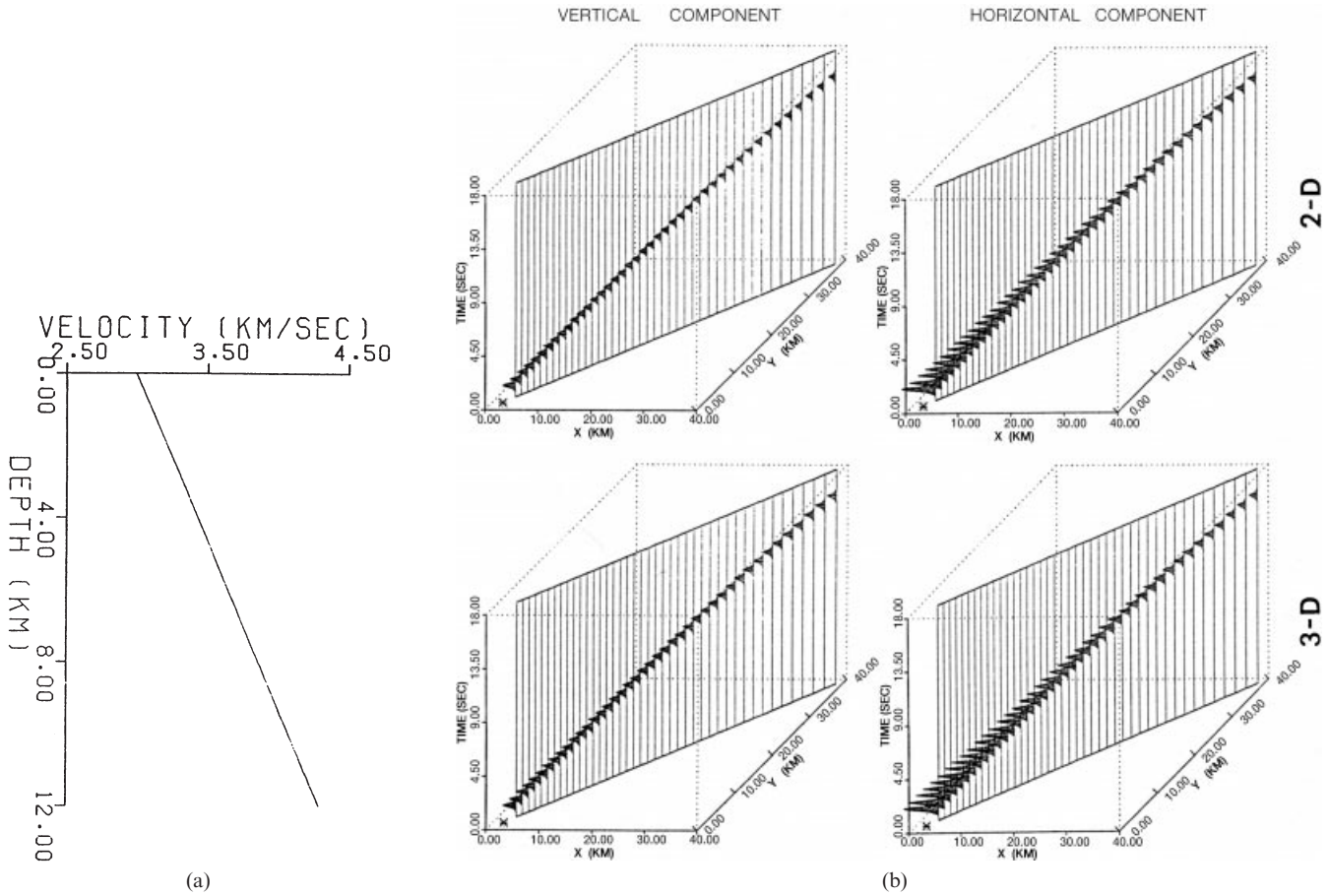

Figure 2. (a) Model, (b) comparison of geometrical synthetic seismograms obtained from different algorithms. The velocity distribution (a) in the model is a linear increase of velocity with depth. The synthetic time profiles [(b), upper panel] were computed using the 2-D algorithm of McMechan & Mooney (1980). The synthetic seismograms [(b), lower panel] were obtained using the 3-D algorithm proposed in this paper. An asterisk denotes the source location.

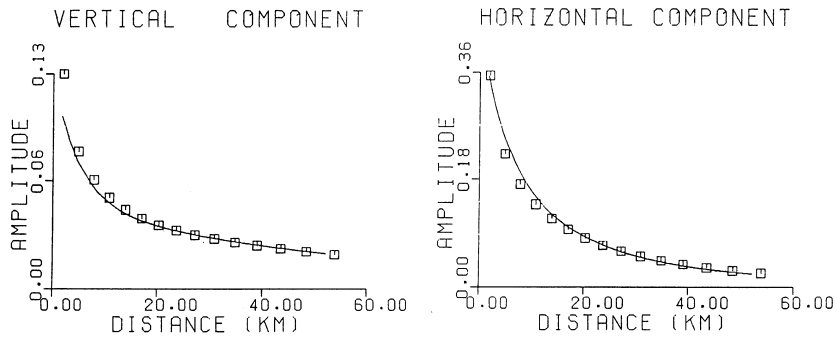

Figure 3. Comparison of amplitude variation as a function of source-to-recorder distance. The amplitude values plotted are from the seismogram profiles shown in Fig. 2. Solid lines and squares correspond to the 2-D and the 3-D algorithms respectively.

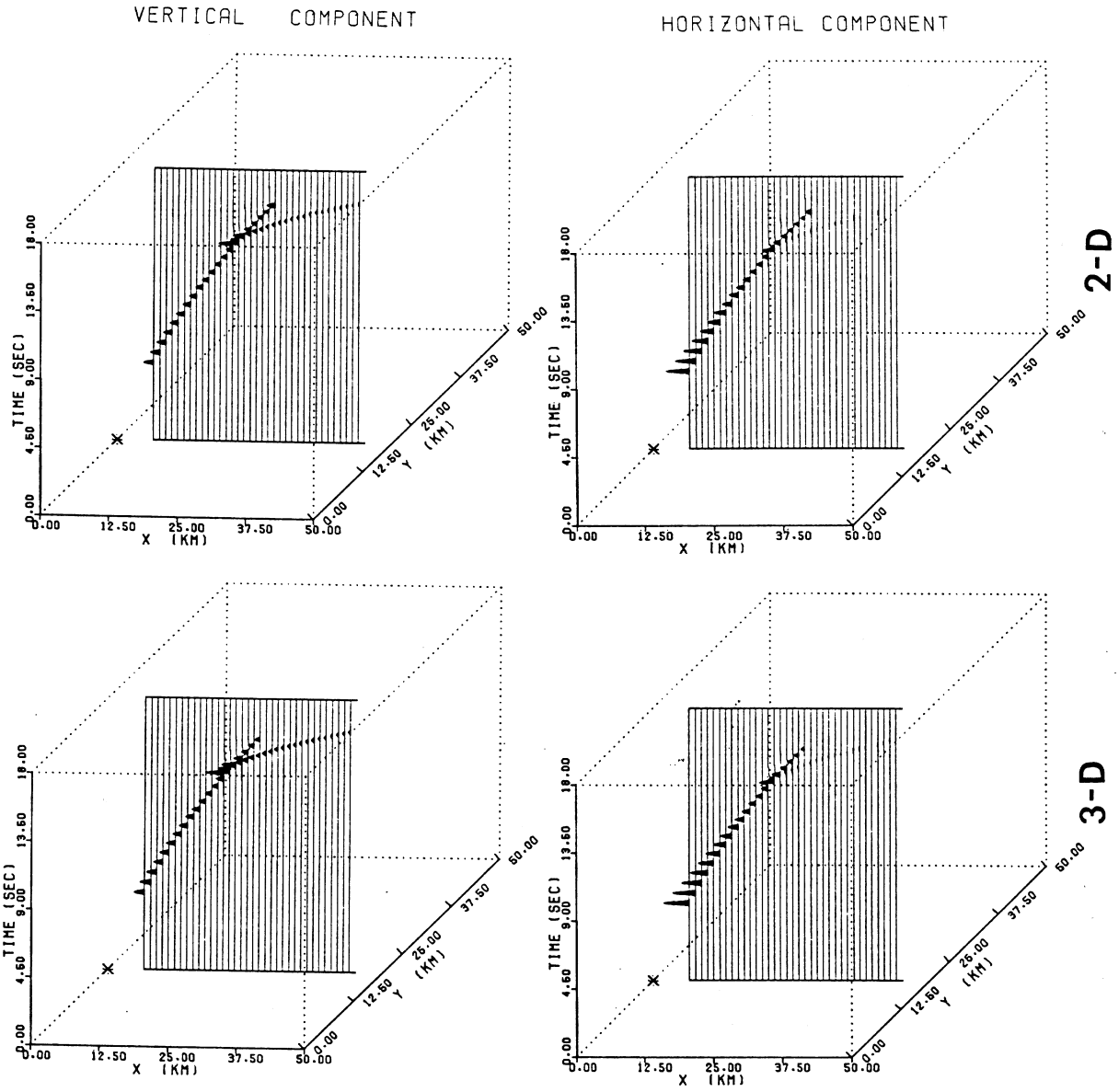

Figure 4. Comparison of synthetic seismograms for a more complicated example. The upper profiles were computed using the 2-D algorithm of McMechan & Mooney (1980); the lower by the 3-D algorithm proposed in this paper. The velocity distribution in the model is a linear increase of velocity with depth. The velocity varies from 3.05 km s^{-1} at the surface to 3.8 km s^{-1} at a depth of 10.0 km and 8.80 km s^{-1} at a depth of 25.0 km. An asterisk denotes the source location.

and transmission coefficients are defined in terms of displacement. The free-surface conversion coefficients are computed, if required. The phase is shifted by $\pi/2$ each time the ray touches an internal caustic. To generate a seismogram for a specified receiver location, a summation is performed of all the rays incident at that location. The seismic wavelet is constructed by a linear combination of a unit impulse with its Hilbert transform (Choy & Richards 1975). Convolving the impulse response with an appropriate apparent source function completes the seismograms.

For each source-to-receiver path, a three-component seismogram (one vertical and two orthogonal horizontal components) can be resolved by decomposing the net amplitude, using the (3-D) angle of incidence at the recorder. The direction of orthogonal decomposition of the horizontal component is arbitrary; obvious choices are north–south and east–west or radial and tangential. To avoid an excessive number of figures, only the net horizontal amplitude is plotted, to present the maximum information within a single plot.

Most seismograms (both synthetic and field data) are displayed here in a 3-D perspective format; each seismogram is plotted against time (t) at the spatial position (x, y) at which it was recorded. This is a direct 3-D extension of the usual 2-D format for a linear recording array where each seismogram is plotted at its source-to-recorder distance.

ALGORITHM TESTING

Before a new algorithm can be used with confidence, it must be tested and compared with existing algorithms. Two types of tests were conducted to test our algorithm. The first was a comparison of the results with the 2-D algorithm of McMechan & Mooney (1980) for a l-D velocity model. This low-level test was of interest because the proposed algorithm is an extension of the McMechan & Mooney framework from 2-D to 3-D; these two algorithms should yield the same solution for l-D and 2-D problems. The second test was a comparison of the results with the 3-D Gaussian-beam algorithm of Červený & Klimeš (1984) for a 3-D velocity model. This test is of interest as the two 3-D methods were developed and implemented independently; production of similar results provides increased confidence in both formulations.

The model (Fig. 2a) employed for the first test was a linear increase of velocity from 3.0 km s^{-1} at 0.0 km to 4.25 km s^{-1} at a depth of 12 km. Fig. 2(b) shows the vertical- and net-horizontal-component seismograms computed for this model using both the 2-D McMechan & Mooney (l980) algorithm and the new 3-D algorithm for an explosive point-source on the Earth's surface. A quantitative comparison (Fig. 3) reveals that the two algorithms yield essentially the same results; minor differences may be attributed to details of implementation of the ray tracing and spreading.

Fig. 4 presents a more complicated model, in which the velocity increases with depth at a rate sufficient for a tripling of the traveltime. The traveltimes in the calculated synthetic seismograms are multivalued functions for certain ranges of source–receiver distance. The multipath problem is alleviated by specifying a different ray group by redefining the initial conditions with a range of azimuth α and take-off angle β, or by shooting a bundle of rays and finding the correct one by interpolation. The traveltime, amplitude and phase behaviour show similar results from both algorithms.

A more realistic 3-D test was performed using the 3-D models and recording geometry of Červený & Klimeš (1984). The velocity model was approximately reconstructed on the basis of the velocity contour profiles presented by them. Synthetic seismograms for a single point-source, for three parallel lines of vertical-component recorders, computed by the Gaussian-beam method of Červený & Klimeš (1984) and by the 3-D geometrical ray theory, are presented in Fig. 5. Except for the usual lack of energy in the pre-cusp region, the new algorithm compares favourably with the Gaussian-beam computations.

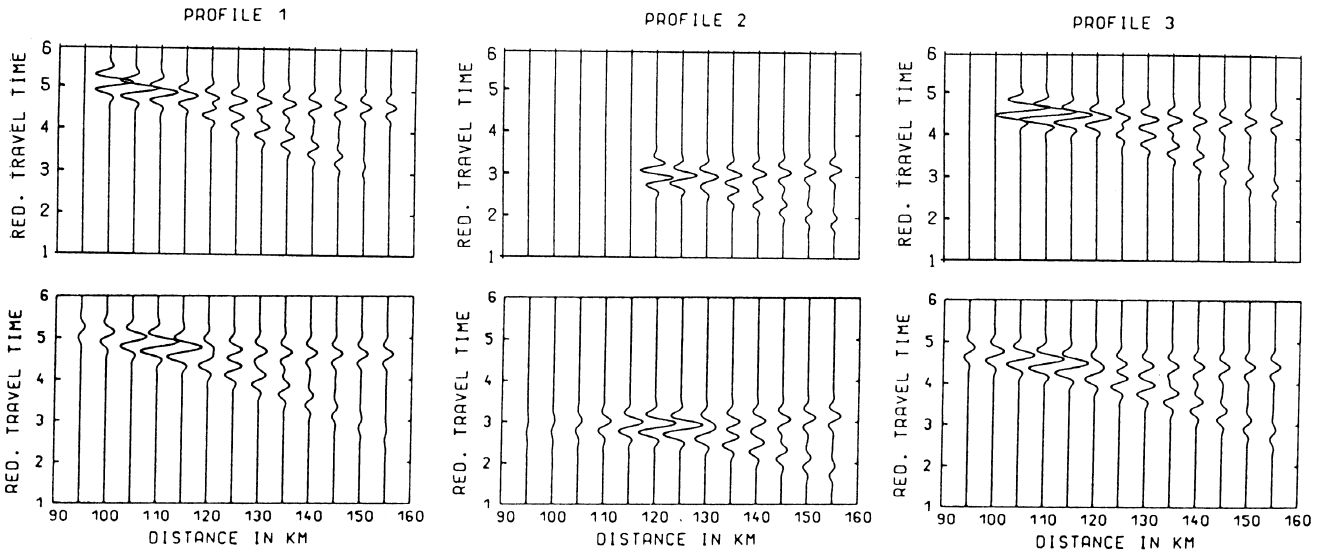

Figure 5. Comparison of Gaussian beams for a 3-D model. The 3-D velocity model for computing synthetic seismograms was taken from Červený & Klimeš (1984). The lower profiles were obtained using the Gaussian-beam approach. The synthetic data were evaluated along three profiles and assumed to have vertical-component recorders on the surface of a 3-D model. The upper profiles are the corresponding output obtained using the geometrical ray tracing algorithm presented in this paper.

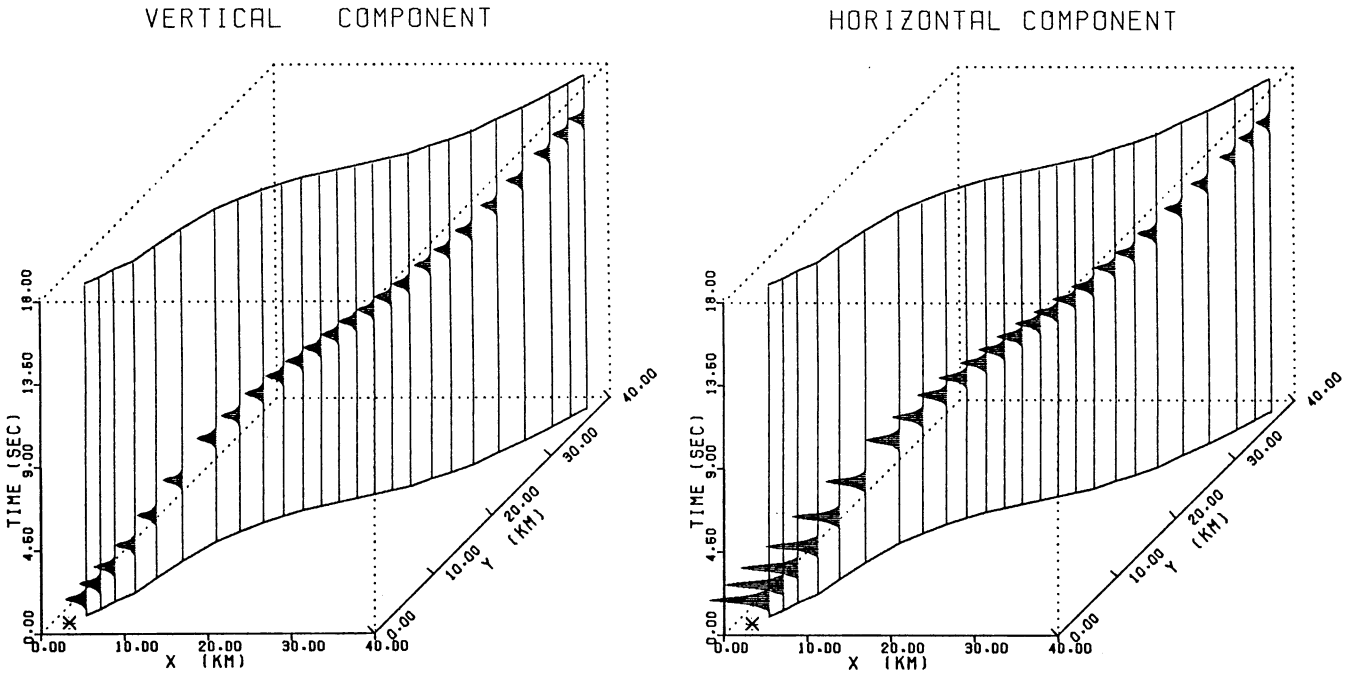

Figure 6. Simulation of seismic data recorded on a typical crooked refraction line with variable recorder spacing. In each panel, the asterisk represents the source location. The velocity model used for generating the seismograms is as shown in Fig. 2(a).

Having shown that the geometrical ray theory produces reliable results (within the limitations of the assumptions involved in the implementation), we apply it to a variety of examples of synthetic and field data.

SYNTHETIC EXAMPLES

One of the main advantages of the present algorithm is its ability to handle arbitrary recording geometries when 3-D effects must be considered. This facilitates modelling of refraction lines, which are typically almost linear, but require projection onto a common line to be processed by 2-D algorithms. Fig. 6 depicts an example in which seismograms with variable spacing along a crooked recording line have been simulated directly in 3-D.

Another geometry that is common, and difficult for displaying data, is earthquake arrays (in which stations are often randomly distributed on the Earth's surface). Large, fixed earthquake-recording arrays usually involve stations in geometrical patterns such as circles or radial lines. Typical recording arrays, especially those designed for measuring wave slowness (such as LASA and NORSAR) or for measuring strong-motion data (such as SMART-1 and SMART-2) can be found throughout the world. Fig. 7 illustrates the latter type, to mimic the pattern of the SMART-1 strong-motion arrays, where a circular recording array overlies a dipping structure.

Fig. 8(a) depicts synthetic seismograms for a source placed at the surface of the model shown in Fig. 7, at $(x, y, z) = (2.0, 2.0, 0.0)$. The asymmetries in time and amplitude are due to the asymmetry of the source and recorders with respect to the structural dip.

All the foregoing examples have considered only *P* waves. If Poisson's ratio is assumed to remain constant and an isotropic radiation pattern for *S* waves is assumed, then a single ray tracer can be used for simulating both of the decoupled *S* and *P* waves. The changes required for constructing seismograms are the substitution of *S*-wave velocities in the model for calculating arrival times, selecting an appropriate *S*-to-*P* energy ratio and *S* directivity for the source, and using the correct geometrical factors for the resolution of the net amplitude into vertical and horizontal components. Fig. 8(b) presents synthetic seismograms containing both *P* and *S* waves from a buried source for the model shown in Fig. 7.

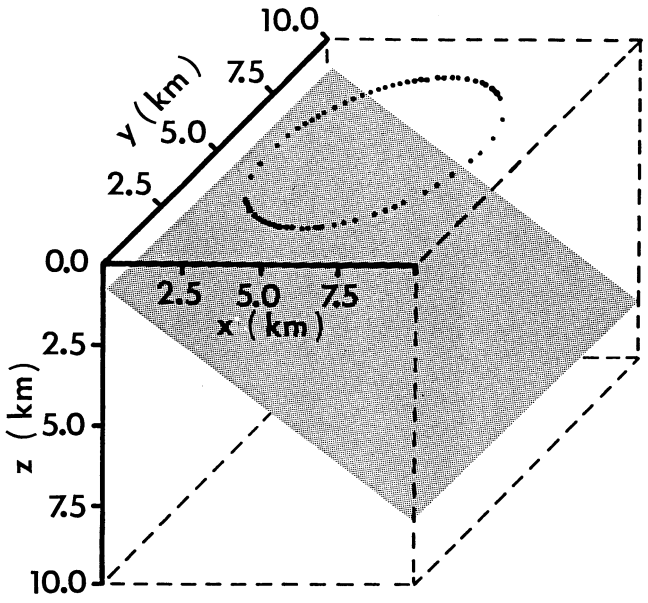

Figure 7. A circular recording array over a dipping structure model used to construct synthetic seismograms. The shaded plane corresponds to a change in velocity gradient. The velocity field within the model increases linearly with depth from 5.6 km s^{-1} at the surface to 7.5 km s^{-1} at the shaded plane, and to 7.7 km s^{-1} at a depth of 10.0 km.

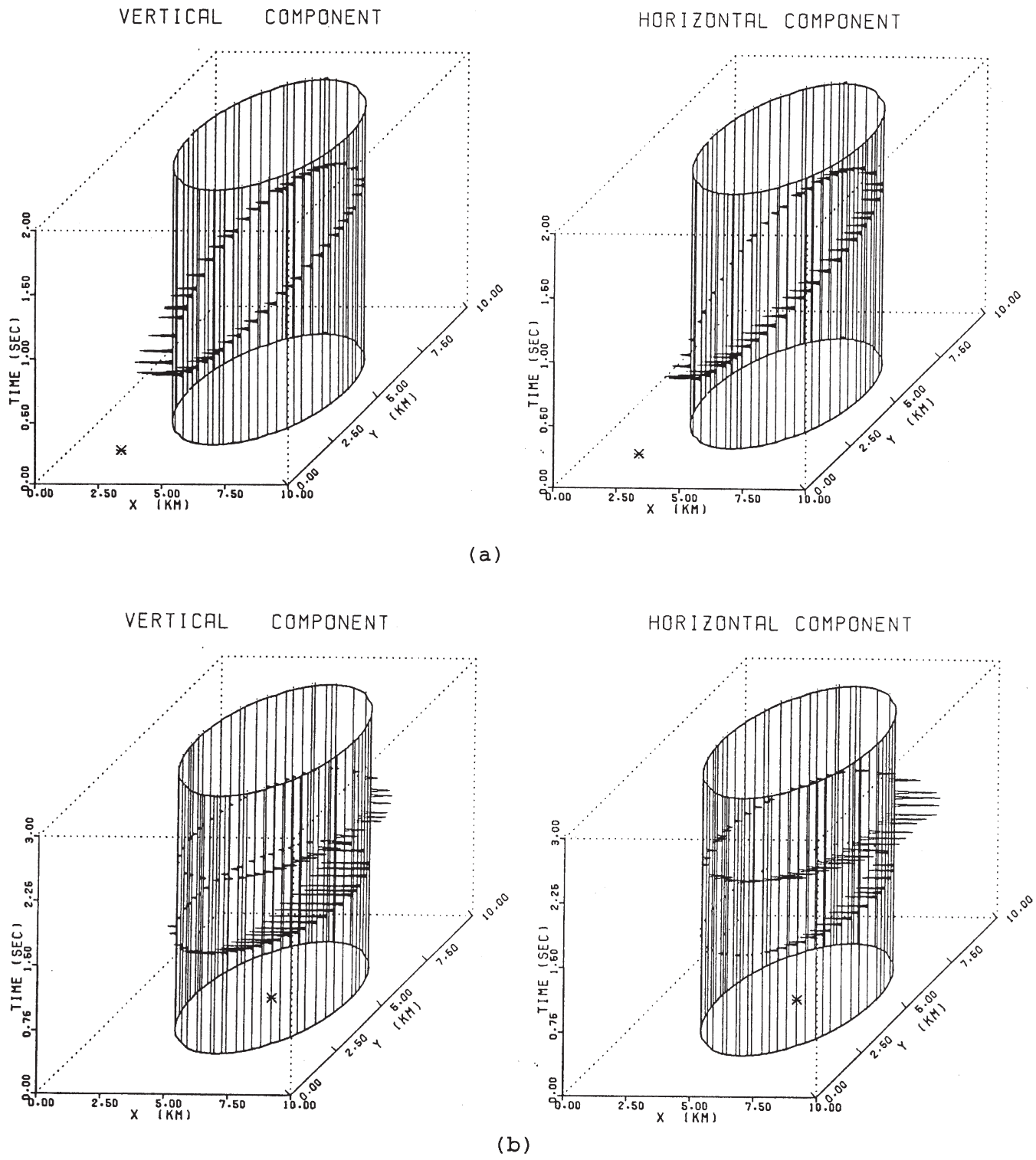

Figure 8. Synthetic seismograms obtained for the model shown in Fig. 7. The asterisk, (a) outside and (b) at the centre of the circle, denotes the epicentre location. Seismic responses for an arbitrary source location are shown. Synthetic seismograms containing *P* waves (a) and both *P* and *S* waves (b) are shown. The source location in (a) is at the surface of the model at $(x, y, z) = (2.0, 2.0, 0.0)$ km. The buried source location in (b) is at $(x, y, z) = (4.5, 4.5, 6.5)$ km. This source lies beneath the shaded plane in Fig. 7.

MODELLING OF FIELD DATA

To illustrate the use of the geometrical 3-D modelling algorithm, a data set recorded at Rainier Mesa at the Nevada Test Site (Ward 1982) was obtained. The reflected energies in these data were previously analysed by Wen & McMechan (1984); the current project was confined to modelling of the transmitted (first-arrival) branch.

The lithological stratigraphic sequences in the study area are a welded tuff layer overlying non-welded tuffs (Fig. 9a). From studies of the area (Gibbons *et al.* 1963) we know that the main reflector is a Palaeozoic dolomite that is overlain by the Piapi Canyon and Indian Trail formations, which are composed of a variety of tuffs (Fig. 9b). Since a detailed geological cross-section is available, an r.m.s. velocity for the tuffs can be fairly accurately estimated from the known depths and the observed traveltimes. The survey geometry (Fig. 10) consists of 17 vibrator locations on the Earth's surface; for each of these, the signal was recorded by 24 recording stations located in a tunnel approximately 457 m beneath the surface. Each station had six 4.5 Hz vertical-component geophones attached to the wall of the tunnel. Thus the recording geometry, as well as the structure, was 3-D. A preliminary velocity

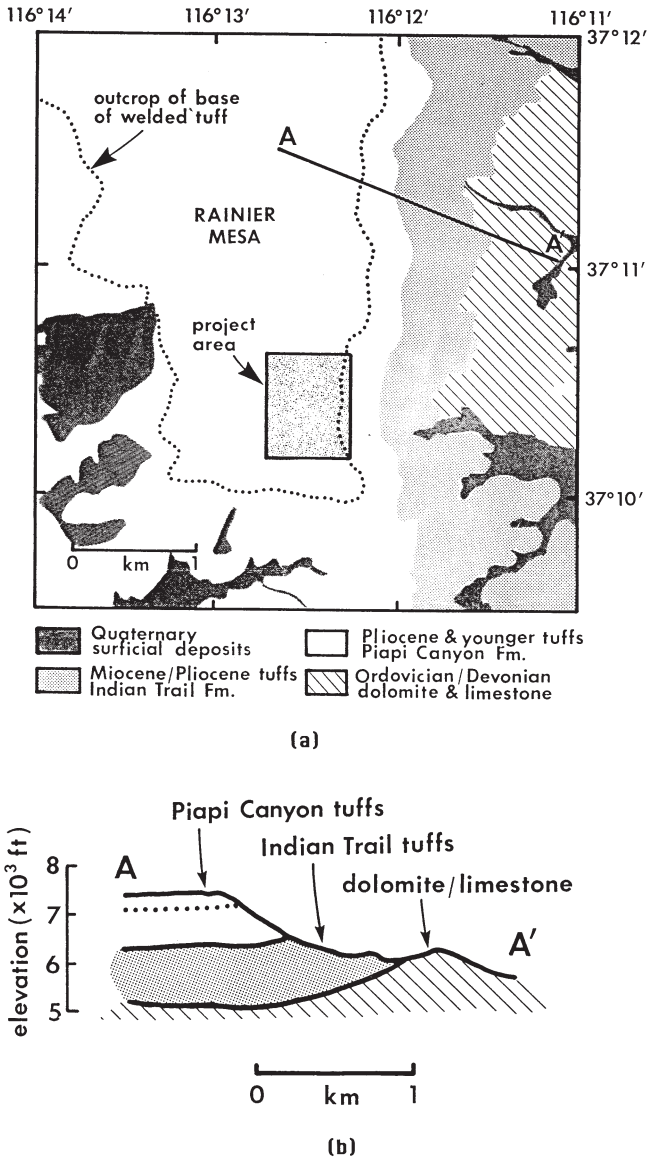

Figure 9. (a) The geology of the Rainier Mesa area of the Nevada Test Site. The location of the seismic survey is indicated by the shaded rectangle. The general shape of the mesa is shown by the dashed line (Wen & McMechan 1984). The corresponding geological cross-section A–A′ is shown in (b). The patterns used to denote geological units are as in (a). The dotted line is the base of the welded tuffs.

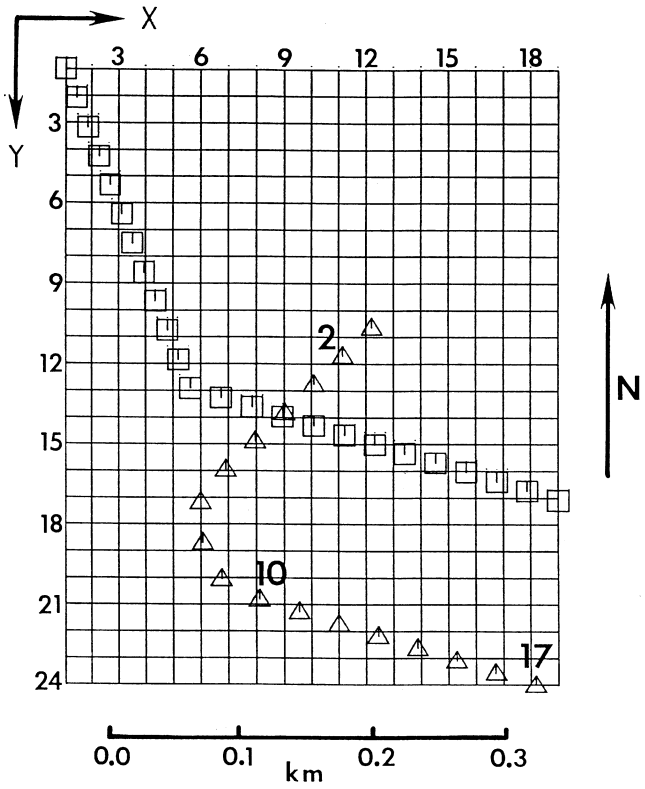

Figure 10. The survey geometry for the vibrator data collected at Rainier Mesa, Nevada Test Site. 17 sources (three of which are numbered) were at the Earth's surface at the locations indicated by the triangles. 24 recorders were placed underground in a tunnel, at the locations indicated by the squares. The signal from each source was recorded at each geophone. The velocity distribution within the project area (Fig. 9) is defined at each grid point.

analysis, using a move-out and stacking process similar to that used in reflection seismology, indicated local lateral-velocity variations of 15 per cent (Table 1). We intended to obtain an estimate of the spatial distribution of these variations by modelling.

Table 1. Velocity estimation for Rainier Mesa, Nevada.

Source number	Time (s)	Velocity (km s^{-1})	Amplitude
1	0.340	1.463	0.224E + 16
2	0.344	1.493	0.294E + 16
3	0.344	1.415	0.351E + 16
4	0.344	1.404	0.402E + 16
5	0.328	1.530	0.230E + 16
6	0.328	1.443	0.128E + 16
7	0.324	1.421	0.338E + 16
8	0.320	1.540	0.298E + 16
9	0.324	1.709	0.908E + 16
10	0.332	1.577	0.105E + 16
11	0.324	1.547	0.270E + 16
12	0.332	1.566	0.284E + 16
13	0.336	1.740	0.320E + 16
14	0.340	1.613	0.325E + 16
15	0.340	1.580	0.228E + 16
16	0.344	1.650	0.220E + 16
17	0.352	1.670	0.207E + 16

The modelling process included iterative ray tracing and computation of synthetic seismograms, comparison of the computed times and amplitudes with the field data, and adjustments of the model. The apparent source wavelet used was derived directly from the data, by stacking over all the move-out-corrected common-source profiles. The radiation pattern for simulating a vertical force was adopted from Aki & Richards (1980). Since the available data for the current 3-D problem are minimal, only an acceptable fit to the field observations can be expected, and an optimum solution cannot be guaranteed. A similar problem would arise if a 3-D travel-time inversion (*cf.* Aki & Lee 1976) using the least-squares approach was attempted.

Fig. 11 illustrates three representative ray paths from each of three source points to all 24 recorders. Refraction of the rays due to the velocity variations is visible. These ray paths are derived from the final velocity model and illustrate, in a qualitative way, the portion of the model that is sampled. Only the central part of the velocity distribution is well constrained. Fig. 12 depicts representative recorded (vertical-component) data and the vertical and horizontal components of the synthetic seismograms produced for the final 3-D velocity distribution. Horizontal and vertical sections of the velocity distributions are shown in Figs 13 and 14 respectively. By assuming a constant Poisson's ratio, the decoupled transmitted *S* waves can be modelled. Traveltimes of *S* waves are obtained from the *P*-wave times, for both the vertical and the horizontal components, by multiplying by 1.783. For display purposes, the amplitudes of the horizontal seismograms have been multiplied by 1.5 relative to the vertical components. Similar fits were obtained for all 17 sources with this velocity model. The traveltimes of *P* waves are fitted to within approximately 0.008 s (two sampling points), and the amplitudes to within approximately 15 per cent of those of the field data. By comparing the synthetic *S*-wave traveltimes with those in the field data, variable time shifts can be observed. This variation in *S*-wave times indicates that Poisson's ratio is not constant, and hence the ray paths for *S* waves are not identical to those for *P* waves. In three dimensions, *S* waves may have two components, *S*1 and *S*2 for the anisotropic case, which are coupled at structure interfaces. Thus, simple scalar multiplication to obtain the *S*-wave velocity from the *P*-wave velocity is not feasible except in certain simple situations. Moreover, the *S* wave may be elliptically polarized. Choosing a reasonable *S*-to-*P* energy ratio at the source and the correct geometrical factor for the resolution of the net amplitude into vertical and horizontal components is also necessary for modelling the amplitudes of *S* waves.

DISCUSSION AND CONCLUSIONS

A geometrical ray theory for computation of synthetic seismograms for 3-D velocity distributions has been implemented. The algorithm is based on traced rays and is a high-frequency approximation. The proposed approach does not predict the energy off the ends of caustics or cusps, as in Gaussian-beam methods, but it compares favourably elsewhere for transmitted energy. Reflection arrivals are not included in the current implementation, although the compression and shear arrivals are included. The current approach for calculating reflection and transmission coefficients is still included explicitly.

The algorithm excludes head waves and higher-order wave phenomena, e.g. diffraction, and is an adequate approximation for most practical applications. Since this is a ray method, it is most accurate when the velocity distribution is a smooth, continuous function in three spatial coordinates. Although the current algorithm is unable to solve the problem of infinite amplitudes predicted for caustics, the algorithm is stable and applicable elsewhere. The approximation for computing the amplitude is advantageous in that the infinite amplitude predicted by classical asymptotic ray theory (ART) for head waves at the critical distance is no longer a difficulty (McMechan & Mooney 1980). Although amplitude and phase information can be modelled, the proposed algorithm still does not give a complete solution for interference, diffraction, absorption and dispersion effects. Further development for the modelling of reflected energy is necessary.

The ray equations allow us to calculate the traveltimes for various refracted paths and the corresponding critical distances beyond which refracted waves still exist. In many instances, the minimum-time path sought for a direct or refracted path satisfying Snell's law is determined by the derivative and the take-off and azimuth angles. The convergence rate depends on the complexity of the model and on the initial conditions.

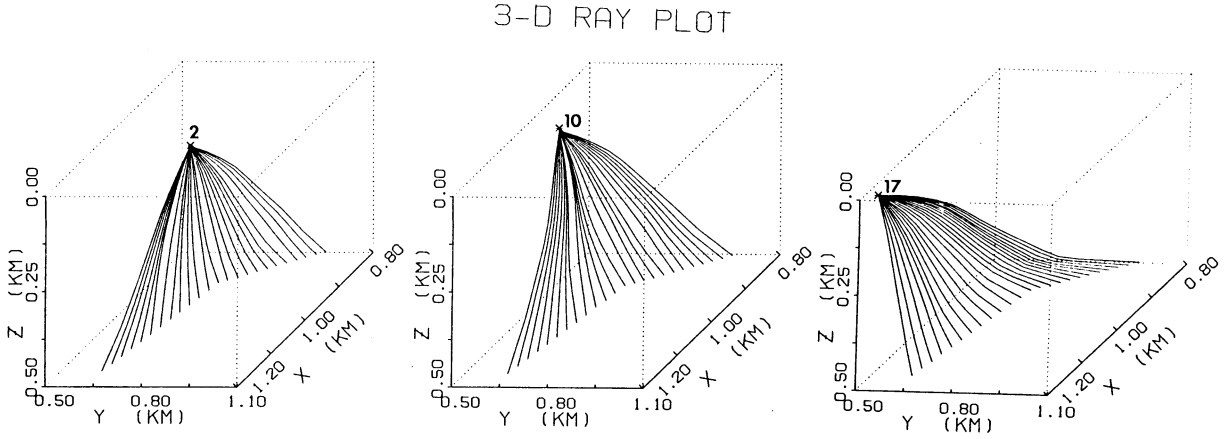

Figure 11. Representative 3-D ray paths through the final velocity model. The paths are for the source locations 2, 10 and 17 shown in Fig. 10. For each source location, there is one ray to each of the 24 underground recorders. Synthetic seismograms computed from these rays are shown in Fig. 12.

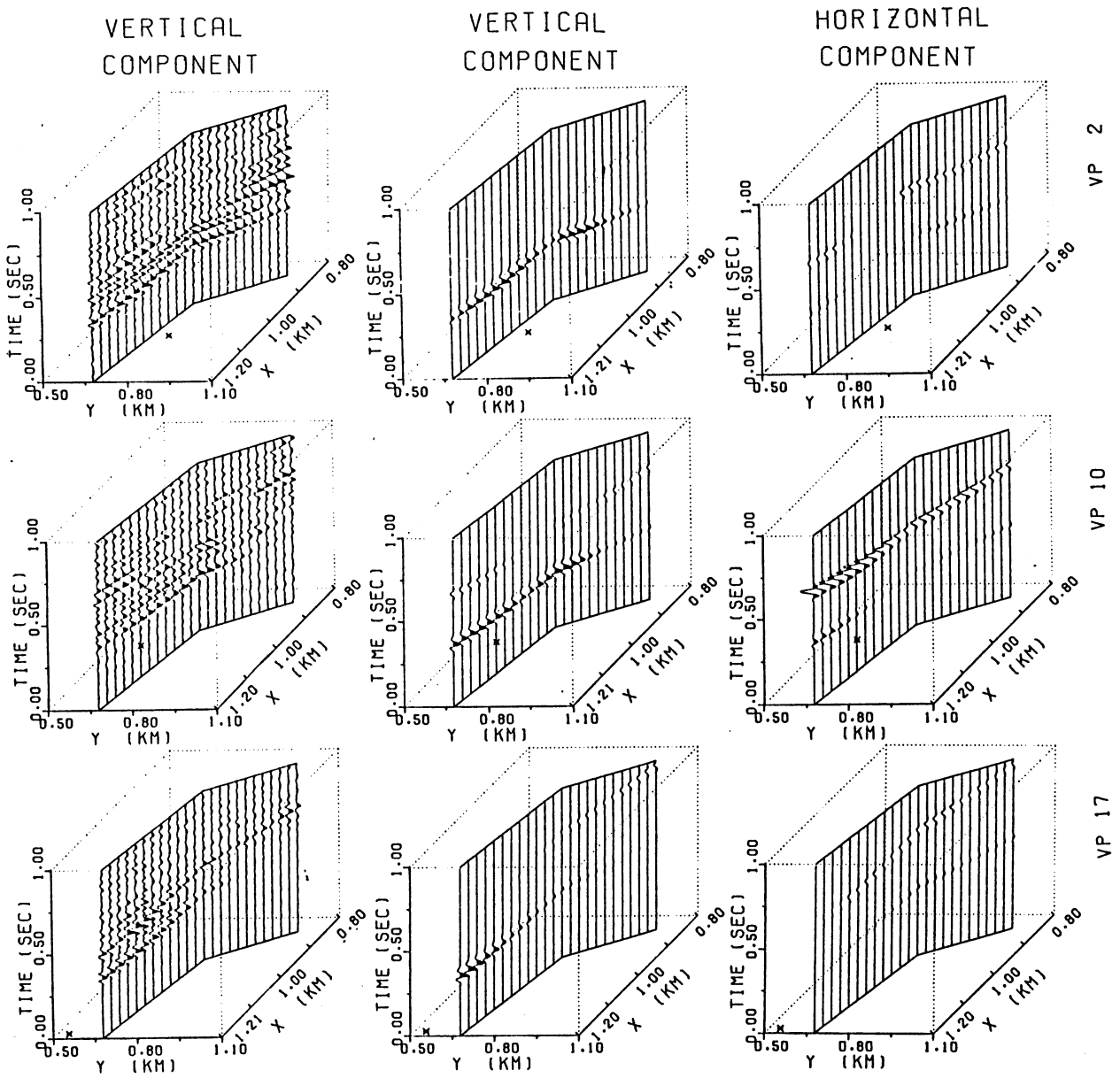

Figure 12. Field and synthetic seismograms containing both *P* and *S* waves. The left column contains the real vertical-component seismograms for source points 2, 10 and 17. Synthetic vertical- and horizontal-component seismograms (computed from the rays in Fig. 11) are shown in the centre and right columns respectively. The amplitudes of the horizontal seismograms are multiplied by 1.5 relative to the vertical seismograms.

In the case of a smoothly varying velocity distribution (as in Fig. 5), the results show that convergence is obtained in fewer than 10 iterations. A receiver continuation strategy is used when searching the ray path for neighbouring receiver positions. For a complex model the traveltime may be multi-valued. The multipath problem may be alleviated by redefining the initial conditions by means of the azimuth α and take-off angle β (i.e. the ray group), or by shooting a bundle of rays and finding the correct one by interpolation. An alternative approach may be to use the 'Fermat ray' instead of the 'Snell ray', as proposed by Waltham (1988), or a point-to-curve ray-tracing method, discussed by Hanyga (1996). The present algorithm may be inefficient for yielding a ray corresponding to the global minimum and may thus fall into a nearby local minimum. However, any converging solution can produce a minimum-traveltime ray path (Julian & Gubbins 1977). A similar restriction can be encountered in a two-point ray-tracing problem based on a three-point perturbation scheme (Um & Thurber 1987).

Our tests of the algorithm with different models show that this procedure yields satisfactory results for 3-D smoothly varying structures. It also considerably decreases the computer time, compared to solving 19 equations simultaneously (seven for ray tracing and 12 for geometrical spreading). Since two additional rays must be traced for the geometrical-spreading calculation, solving 7×3 differential equations is necessary. However, the number of arithmetic operations required for eqs (A3) is significantly less than for the dynamic ray-tracing algorithm given in Appendix B [see expressions for $\dot{W}_7$–$\dot{W}_{18}$ in eqs (B3)]. Parallel implementation of the proposed algorithm

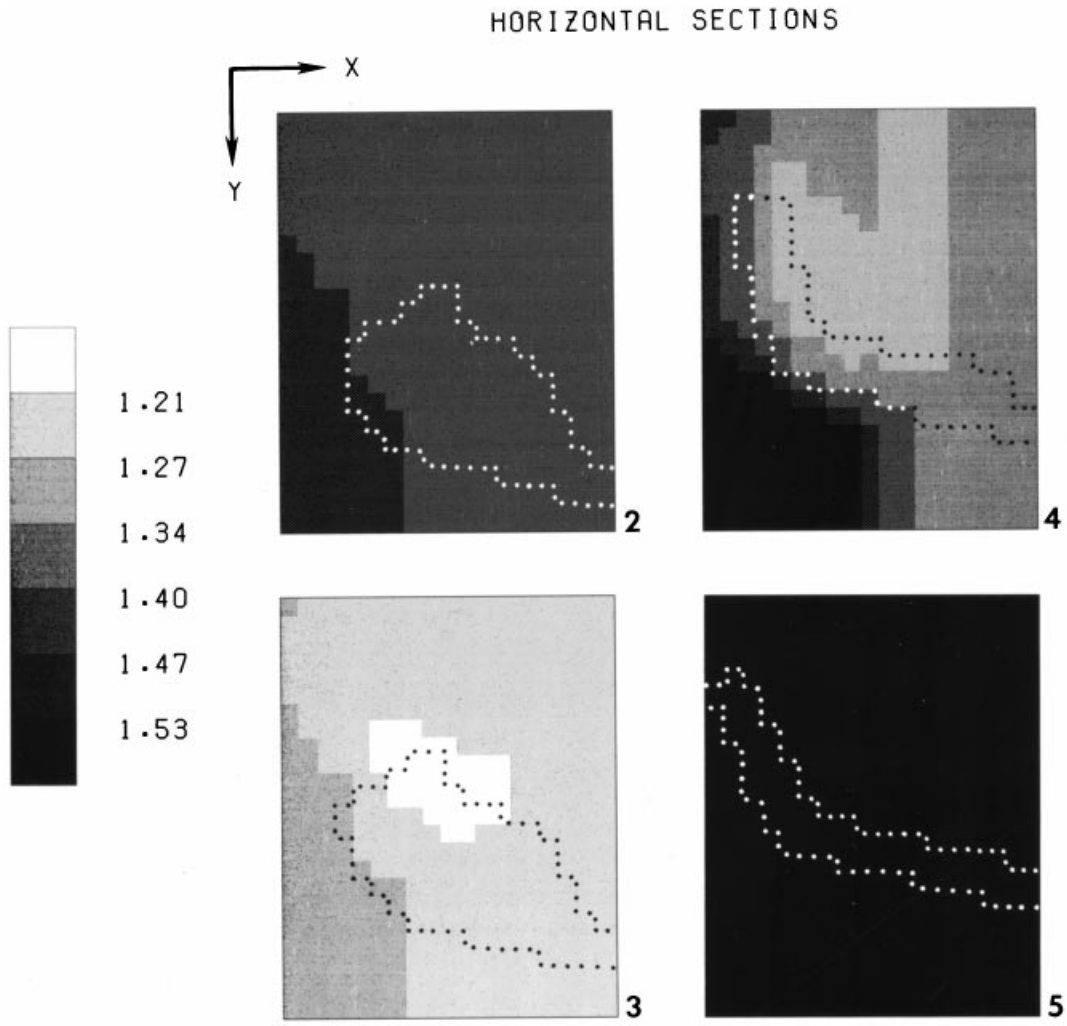

Figure 13. Representative horizontal sections through the 3-D Nevada Test Site velocity model. Slice 2 is at 96 m depth; 3, 152 m, 4, 343 m; and 5, 400 m. The numbers on the grey scale denote velocities in km s^{-1}.

and developing a parallel code for solving partial differential equations, as was designed for the dynamic ray equations in eqs (B3), on a massively-parallel-processor computer will improve both schemes accurately and efficiently (*cf*. Kao & Chen 1996).

In the conventional 2-D algorithm applied to actual 3-D field data, it is always assumed that the seismic energy is confined in the plane of the 2-D structure profile. For field data records, the transmitted and reflected seismic energy is obtained from in-plane as well as from out-of-plane paths. The recorded seismic responses are strongly related to subsurface structure and source–receiver geometry. The major advantage of the current algorithm is its flexibility in modelling diverse source and recorder configurations, e.g. crooked refraction lines and circular arrays. This method has been successfully applied to 3-D modelling of seismic waves transmitted from surface vibrator sources to receivers located in a tunnel at Rainier Mesa, Nevada.

For the current 3-D problem, the available data are minimal owing to the finite recording aperture, so that only an acceptable fit to the field observations is expected, with no guarantee that the model obtained is the optimal solution. The estimated velocity structure is still a simplified solution, owing to insufficient sampling of the velocity field by the ray paths. A similar problem would arise if a 3-D traveltime inversion was attempted using the least-squares method (*cf*. Aki & Lee 1976).

ACKNOWLEDGMENTS

The author is very indebted to Dr Robert P. Comer for initiating the 3-D seismic ray tracing scheme and for many valuable suggestions. Technical support and suggestions from George A. McMechan contributed significantly to the research in this paper. The data were collected by the University of Texas at Dallas (UTD) in conjunction with Los Alamos National Laboratory (LANL). The seismic data were prepared by Joe Nation of UTD. The author is also grateful to two anonymous reviewers for carefully reading this paper and for their constructive and valuable comments on the manuscript. This research was supported in part by the National Science Council under grant number NSC-886-21 16-M-194-002-Y, the sponsors of the Petroleum Research Fund of the American Chemical Society under contract number 1 8721 5-AC2 and by the National Science Foundation under grant number EAR-8605999.

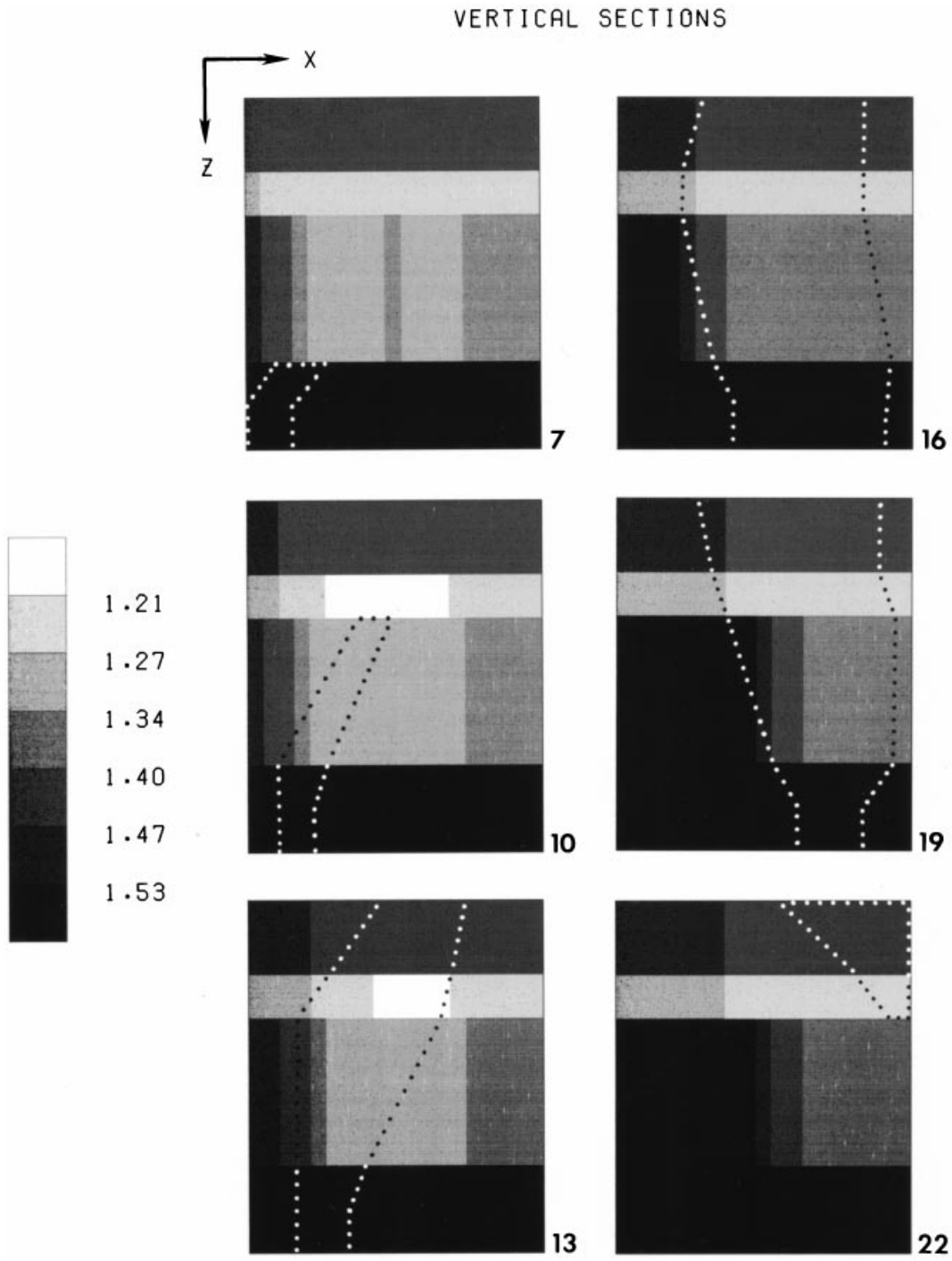

Figure 14. Representative vertical sections through the 3-D Nevada Test Site velocity model. The number at the lower right corner of each section denotes the corresponding (fixed-*y*) position of the section in Fig. 10. The numbers on the grey scale denote velocities in km s^{-1}.

REFERENCES

Aki, K. & Lee, W.H.K., 1976. Determination of three-dimensional velocity anomalies under a seismic array using first *P* arrival times from local earthquakes, I. A homogeneous initial model, *J. geophys. Res.,* **81,** 4381–4399.

Aki, K. & Richards, P., 1980. *Quantitative Seismology: Theory and Methods,* W.H. Freeman, San Francisco, CA.

Azbel, I.Ya., Dmitrieva, L.A., Gobarenko, V.S. & Yanovskaya, T.B., 1984. Numerical modelling of wavefields in three-dimensional inhomogeneous media, *Geophys. J. R. astr. Soc.,* **79,** 199–206.

Bard, P. & Bouchon, M., 1980a. The seismic response of sediment-filled valleys. Part I. The case of incident *SH* waves, *Bull. seism. Soc. Am.,* **70,** 1263–1286.

Bard, P. & Bouchon, M., 1980b. The seismic response of sediment-filled valleys. Part II. The case of incident *P-SV* waves, *Bull. seism. Soc. Am.,* **70,** 1921–1941.

Beydoun, W.B. & Keho, T.H., 1987. The paraxial ray method, *Geophysics,* **52,** 1639–1653.

Bulant, P., 1996. Two-point ray tracing in 3-D, *Pure appl. Geophys.,* **148,** 421–447.

Burdick, L.J. & Salvado, C.A., 1986. Modeling body wave amplitude

fluctuations using the three-dimensional slowness method, *J. geophys. Res.,* **91,** 12 483–12 496.
Cao, S. & Greenhalgh, S., 1993. Calculation of the seismic first-break time, field and its ray path distribution using a minimum traveltime tree algorithm, *Geophys. J. Int.,* **114,** 593–600.
Červený, V. & Hron, F., 1980. The ray series method and dynamic ray tracing systems for 3-D inhomogeneous media, *Bull. seism. Soc. Am.,* **70,** 47–77.
Červený, V. & Klimeš, L., 1984. Synthetic body wave seismograms for three-dimensional laterally varying media, *Geophys. J. R. astr. Soc.,* **79,** 119–133.
Červený, V. & Pšenčík, I., 1983. Gaussian beams and paraxial ray approximation in three-dimensional elastic inhomogeneous media, *J. Geophys.,* **53,** 1–15.
Červeńy, V. & Rarindra, R., 1971. *Theory of Seismic Head Waves,* University of Toronto Press, Toronto.
Červený, V., Klimeš, L. & Pšenčík, I., 1988. Applications of dynamic ray tracing, *Phys. Earth planet. Inter.,* **51,** 25–35.
Chapman, C.H., 1978. A new method for computing synthetic seismograms, *Geophys. J. R. astr. Soc.,* **54,** 481–518.
Choy, G.L. & Richards, P.G., 1975. Pulse distortion and Hilbert transformation in multiple reflected and refracted body waves, *Bull. seism. Soc. Am.,* **65,** 55–70.
Dellinger, J., 1991. Anisotropic finite-difference traveltimes, in *Expanded Abstracts, 61st Ann. Int. SEG Meeting,* pp. 1530–1533.
Dijkstra, E., 1959. A note on two problems in connection with graphs, *Numer. Math.,* **I,** 269–271.
Ettrich, N. & Gajewaki, D., 1996. Wave front construction in smooth media for prestack depth migration, *Pure appl. Geophys.,* **148,** 481–502.
Fischer, R. & Lees, J., 1993. Shortest path ray tracing with sparse graphs, *Geophysics,* **58,** 987–996.
Frazer, L.N. & Phinney, R.A., 1980. The theory of finite frequency body wave synthetic seismograms in inhomogeneous elastic media, *Geophys. J. R. astr. Soc.,* **63,** 691–717.
Gibbons, A., Hindricks, E., Hanson, W. & Lemke, R., 1963. *Geologic Map of the Rainier Mesa Quadrangle, Nye County, Nevada,* Exploration Services Division, Geosource, Inc., Houston, Texas.
Hanyga, A., 1988. Numerical method of tracing rays and wave fronts, in *Seismological Algorithms,* Academic Press, New York, NY.
Hanyga, A., 1996. Point-to-curve ray tracing, *Pure appl. Geophys.,* **148,** 387–420.
Hilterman, F.J., 1970. Three-dimensional seismic modelling, *Geophysics,* **35,** 1020–1037.
Julian, B.R. & Gubbins, D., 1977. Three-dimensional seismic ray tracing, *J. Geophys.,* **43,** 95–113.
Kao, J.C. & Chen, H.W., 1996. Massively parallel computing of shortest raypath and traveltime in 2-D and 3-D models, *Terrest. atmos. ocean. Sci.,* **7,** 299–315.
Kennett, B.L.N., 1983. *Seismic Wave Propagation in Stratified Media,* Cambridge University Press, Cambridge.
Klimeš, L. & Kvasnicka, M., 1994. 3-D network ray tracing, *Geophys. J. Int.,* **116,** 726–738.
Lee, W.H.K. & Stewart, S.W., 1981. *Principles and Applications of Microearthquake Networks,* Academic Press, New York, NY.
May, B.T. & Hron, H., 1978. Synthetic seismic sections of typical petroleum traps, *Geophysics,* **43,** 1119–1147.
McMechan, G.A. & Mooney, W.D., 1980. Asymptotic ray theory and synthetic seismograms for laterally varying structures: theory and application to the Imperial Valley, California, *Bull. seism. Soc. Am.,* **70,** 2021–2035.
McMechan, G.A., Wen, J. & Morales, J.A., 1988. 3-D acoustic modelling and imaging for earthquake data, *Geophys. J. R. astr. Soc.,* **92,** 339–344.
Mikhailenko, B.G., 1984. Synthetic seismograms for complex three-dimensional geometries using an analytical–numerical algorithm, *Geophys. J. R. astr. Soc.,* **79,** 963–986.
Moser, T., 1991. Shortest path calculation of seismic rays, *Geophysics,* **56,** 59–67.
Mufti, I.R., 1990. Large-scale three-dimensional seismic models and their interpretive significance, *Geophysics,* **55,** 1166–1182.
Nakanishi, I. & Yamaguchi, K., 1986. A numerical experiment on nonlinear image reconstruction from first-arrival times for two-dimensional island arc structure, *J. Phys. Earth,* **34,** 195–201.
Pereyra, V., 1992. Two-point ray tracing in general 3D media, *Geophys. Prospect.,* **40,** 267–287.
Pereyra, V., 1996. Modeling, ray tracing, and block nonlinear traveltime inversion in 3-D, *Pure appl. Geophys.,* **148,** 345–386.
Pereyra, V., Lee, W.H.K. & Keller, H.S., 1980. Solving two-point seismic ray-tracing problems in a heterogeneous medium. Part 1. A general adaptive finite-difference method, *Bull. seism. Soc. Am.,* **70,** 79–99.
Podvin, P. & Lecomte, I., 1991. Finite-difference computation of traveltimes in very contrasted velocity models: a massively parallel approach and its associated tools, *Geophys. J. Int.,* **105,** 271–284.
Qin, F., Luo, Y., Olsen, K., Cai, W. & Schuster, G., 1992. Finite-difference solution of the eikonal equation along expanding wavefronts, *Geophysics,* **57,** 478–487.
Reshef, M. & Kosloff, D., 1986. Migration of common-shot gathers, *Geophysics,* **51,** 324–331.
Saito, H., 1989. Traveltimes and raypaths of first arrival seismic waves: computation method based on Huygens' principle, in *Expanded Abstracts, 59th Ann. Int. SEG Meeting,* pp. 244–247.
Saito, H., 1990. 3-D ray-tracing method based on Huygens' principle, in *Expanded Abstracts, 60th Ann. Int. SEG Meeting,* pp. 1024–1027
Shampine, L.F. & Gordon, M.K., 1975. *Computer Solution of Ordinary Differential Equations: the Initial Value Problem,* Freeman, San Francisco, CA.
Sinton, J.B. & Frazer, L.N., 1982. A method for computation of finite-frequency body wave synthetic seismograms, *Geophys. J. R. astr. Soc.,* **71,** 37–55.
Smith, W.R., 1975. The application of finite element analysis to body wave propagation problems, *Geophys. J. R. astr. Soc.,* **42,** 747–768.
Trorey, A.W., 1970. A simple theory for seismic diffractions, *Geophysics,* **35,** 762–784.
Um, J. & Thurber, C., 1987. A fast algorithm for two-point seismic ray tracing, *Bull. seism. Soc. Am.,* **77,** 972–986.
Van Trier, J. & Symes, W.W., 1991. Upwind finite-difference calculation of traveltimes, *Geophysics,* **56,** 812–821.
Vidale, J., 1988. Finite-difference calculation of traveltimes, *Bull. seism. Soc. Am.,* **78,** 2062–2076.
Vidale, J., 1990. Finite-difference calculation of traveltimes in three dimensions, *Geophysics,* **55,** 521–526.
Vinje, V., Iversen, E. & Gjoystdal, H., 1993. Traveltime and amplitude estimation using wave front construction, *Geophysics,* **58,** 1157–1166.
Ward, R.W., 1982. Surface to tunnel seismic transmission measurements at the Nevada Test Site, *Final report on contract No. 9-L12-D9122-1 to Los Alamos National Laboratory.*
Waltham, D.A., 1988. Two-point ray tracing using Fermat's principle, *Geophys. J.,* **93,** 575–5882.
Wen, J. & McMechan, G.A., 1984. Application of three-dimensional kinematic imaging to analysis of seismic reflection data from the Nevada Test Site, *Bull. seism. Soc. Am.,* **74,** 2187–2199.
Wesson, R.L., 1970. A time integration method for computation of the intensities of seismic rays, *Bull. seism. Soc. Am.,* **60,** 307–316.

APPENDIX A: THE 3-D KINEMATIC RAY TRACING

This appendix contains a summary of the standard seismic ray-tracing algorithm for heterogeneous, isotropic, 3-D media. Details of the derivation can be found in Lee & Stewart (1981). From the eikonal (image) equation, we can derive the ray

equation, which is a second-order ordinary differential equation (ODE) governing the ray path:

$$\frac{d}{ds}\left(\frac{1}{v}\frac{d\mathbf{r}}{ds}\right)=\nabla\left(\frac{1}{v}\right), \tag{A1}$$

where $d\mathbf{r}=[x(s), y(s), z(s)]$ and $v(x, y, z)$ is the local wave velocity. The velocity is a function of the spatial position vector $\mathbf{r}$ and s is an independent variable representing the path length along the ray. The term $d\mathbf{r}/ds$ is the tangent vector (with unit length) and ∇ is the gradient operator. The ray equations may also be derived from Fermat's principle of minimum (or maximum) time.

Any system of second-order ordinary differential equations can be reduced to a system of first-order equations by defining the slowness vector $\mathbf{P}(s)$ such that $\mathbf{P}=(P_x, P_y, P_z)=(1/v)(d\mathbf{r}/ds)$. Then,

$$\frac{d\mathbf{r}}{ds}=v\mathbf{P},$$

$$\frac{d\mathbf{P}}{ds}=\nabla\left(\frac{1}{v}\right), \tag{A2}$$

with six components. Eq. (A2) is equivalent to the original second-order system with three components. To keep track of the traveltime $t(s)$ we may add a seventh equation $dt/ds=1/v$. So, in the Cartesian coordinate system, eq. (A1) can be decomposed into seven ODEs by setting $U=1/v$, $P_x=\mathrm{U}(dx/ds)=W_2$, $P_z=U(dz/ds)=W_6$, $x=W_1$, $y=W_3$, $z=W_5$, $t=W_7$ and $\mathbf{P}=(W_2, W_4, W_6)$, where (W_2, W_4, W_6) are the x, y and z components of the slowness vector, such that eq. (A2) becomes

$$\begin{aligned}
&W_1=x, && \dot{W}_1=vW_2,\\
&W_2=U\dot{x}, && \dot{W}_2=U_x,\\
&W_3=y, && \dot{W}_3=vW_4,\\
&W_4=U\dot{y}, && \dot{W}_4=U_y,\\
&W_5=z, && \dot{W}_5=vW_6,\\
&W_6=U\dot{z}, && \dot{W}_6=U_z,\\
&W_7=t, && \dot{W}_7=U.
\end{aligned} \tag{A3}$$

The dot denotes differentiation with respect to the path length s. These seven equations are solved simultaneously for $\dot{W}_1$–$\dot{W}_7$ by a Runge–Kutta–Felberg (4, 5) algorithm.

APPENDIX B: THE 3-D DYNAMIC RAY TRACING

The dynamic ray-tracing algorithm is an alternative approach to the evaluation of high-frequency seismic wavefields to compute the seismic ray amplitude and other quantities, such as wave-front curvature, in laterally inhomogeneous, isotropic media. A straightforward approach to describe the initial direction of a ray is to specify the azimuth (α) and take-off (β) angles (Fig. B1). These are defined such that at the initial point (source location) $\dot{x}=\cos\alpha\sin\beta$, $\dot{y}=\sin\alpha\sin\beta$ and $\dot{z}=\cos\beta$. As the first step in obtaining the derivatives required to speed the convergence of the shooting approach, we derive differential equations for the quantities $\partial x(s)/\partial\alpha$, $\partial y(s)/\partial\alpha$, $\partial z(s)/\partial\alpha$ and $\partial x(s)/\partial\beta$, $\partial y(s)/\partial\beta$, $\partial z(s)/\partial\beta$ in terms of the path length s. For example, by applying the chain rule $(d/ds)(\partial x/\partial\alpha)$, the equation

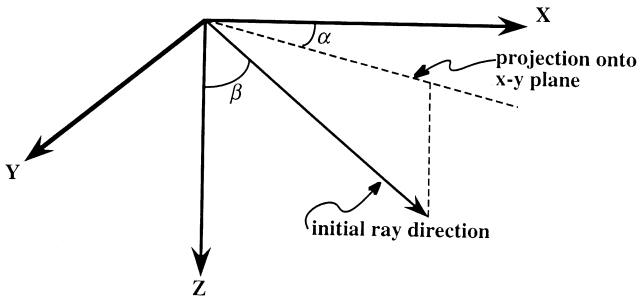

Figure B1. Ray coordinates.

becomes

$$\frac{d}{ds}\left(\frac{\partial x}{\partial\alpha}\right)=\frac{\partial}{\partial\alpha}(vW_2)=W_2\left(v_x\frac{\partial x}{\partial\alpha}+v_y\frac{\partial y}{\partial\alpha}+v_z\frac{\partial z}{\partial\alpha}\right)+v\frac{\partial W_2}{\partial\alpha}. \tag{B1}$$

The new quantity $\partial W_2/\partial\alpha$ also satisfies a differential equation,

$$\frac{d}{ds}\left(\frac{\partial W_2}{\partial\alpha}\right)=\frac{\partial}{\partial\alpha}(\dot{W}_2)=\frac{\partial}{\partial\alpha}(U_x)=U_{xx}\frac{\partial x}{\partial\alpha}+U_{xy}\frac{\partial y}{\partial\alpha}+U_{xz}\frac{\partial z}{\partial\alpha}. \tag{B2}$$

Equations such as eqs (Bl) and (B2) may be obtained for all six combinations of α or β with x, y or z, so that we may add 12 equations to the system in eqs (A3) to yield a new system of 19 first-order ordinary differential equations. If we define the set of dependent variables $W_1, W_2, W_3, \ldots, W_{19}$, the system and corresponding definitions are

$$\begin{aligned}
&W_1=x, && \dot{W}_1=vW_2,\\
&W_2=U\dot{x}, && \dot{W}_2=U_x,\\
&W_3=y, && \dot{W}_3=vW_4,\\
&W_4=U\dot{y}, && \dot{W}_4=U_y,\\
&W_5=z, && \dot{W}_5=vW_6,\\
&W_6=U\dot{z}, && \dot{W}_6=U_z,\\
&W_7=\frac{\partial x}{\partial\alpha}=\frac{\partial W_1}{\partial\alpha}, && \dot{W}_7=(v_xW_7+v_yW_9+v_zW_{11})W_2+vW_8,\\
&W_8=\frac{\partial W_2}{\partial\alpha}, && \dot{W}_8=U_{xx}W_7+U_{xy}W_9+U_{xz}W_{11},\\
&W_9=\frac{\partial y}{\partial\alpha}=\frac{\partial W_3}{\partial\alpha}, && \dot{W}_9=(v_xW_7+v_yW_9+v_zW_{11})W_4+vW_{10},\\
&W_{10}=\frac{\partial W_4}{\partial\alpha}, && \dot{W}_{10}=U_{yx}W_7+U_{yy}W_9+U_{yz}W_{11},\\
&W_{11}=\frac{\partial z}{\partial\alpha}=\frac{\partial W_5}{\partial\alpha}, && \dot{W}_{11}=(v_xW_7+v_yW_9+v_zW_{11})W_6+vW_{12},\\
&W_{12}=\frac{\partial W_6}{\partial\alpha}, && \dot{W}_{12}=U_{zx}W_7+U_{zy}W_9+U_{zz}W_{11},\\
&W_{13}=\frac{\partial x}{\partial\beta}=\frac{\partial W_1}{\partial\beta}, && \dot{W}_{13}=(v_xW_{13}+v_yW_{15}+v_zW_{17})W_2+vW_{14},\\
&W_{14}=\frac{\partial W_2}{\partial\beta}, && \dot{W}_{14}=U_{xx}W_{13}+U_{xy}W_{15}+U_{xz}W_{17},
\end{aligned}$$

$$W_{15} = \frac{\partial y}{\partial \beta} = \frac{\partial W_3}{\partial \beta}, \quad \dot{W}_{15} = (v_x W_{13} + v_y W_{15} + v_z W_{17}) W_4 + v W_{16},$$

$$W_{16} = \frac{\partial W_4}{\partial \alpha}, \quad \dot{W}_{16} = U_{yx} W_{13} + U_{yy} W_{15} + U_{yz} W_{17},$$

$$W_{17} = \frac{\partial z}{\partial \beta} = \frac{\partial W_5}{\partial \beta}, \quad \dot{W}_{17} = (v_x W_{13} + v_y W_{15} + v_z W_{17}) W_6 + v W_{18},$$

$$W_{18} = \frac{\partial W_6}{\partial \beta}, \quad \dot{W}_{18} = U_{zx} W_{13} + U_{zy} W_{15} + U_{zz} W_{17},$$

$$W_{19} = t, \quad \dot{W}_{19} = U, \tag{B3}$$

and, as in eqs (A3), a dot denotes differentiation with respect to the path length s. The appropriate initial conditions for this system of equations, corresponding to a ray starting at the point (x_0, y_0, z_0) with $s = 0$ and azimuth and take-off angles α and β respectively are

$$W_1(0) = x_0,$$
$$W_2(0) = u_0 \cos\alpha \sin\beta,$$
$$W_3(0) = y_0,$$
$$W_4(0) = u_0 \sin\alpha \sin\beta,$$
$$W_5(0) = z_0,$$
$$W_6(0) = u_0 \cos\beta,$$
$$W_7(0) = 0,$$
$$W_8(0) = -u_0 \sin\alpha \sin\beta,$$
$$W_9(0) = 0,$$
$$W_{10}(0) = u_0 \cos\alpha \sin\beta,$$
$$W_{11}(0) = 0,$$
$$W_{12}(0) = 0,$$
$$W_{13}(0) = 0,$$
$$W_{14}(0) = u_0 \cos\alpha \cos\beta,$$
$$W_{15}(0) = 0,$$
$$W_{16}(0) = u_0 \sin\alpha \cos\beta,$$
$$W_{17}(0) = 0,$$
$$W_{18}(0) = -u_0 \sin\beta,$$
$$W_{19}(0) = 0, \tag{B4}$$

where $u_0 = u(x_0, y_0, z_0)$.